

REVISITING THE IRON ABUNDANCE IN THE HYPER IRON-POOR STAR HE 1327–2326
WITH UV COS/*HST* DATA*

RANA EZZEDDINE^{1,2} AND ANNA FREBEL^{2,1}

¹*Joint Institute for Nuclear Astrophysics - Center for Evolution of the Elements (JINA-CEE), USA*

²*Department of Physics & Kavli Institute for Astrophysics and Space Research, Massachusetts Institute of Technology, Cambridge, MA 02139, USA*

(Received May 2018; Revised; Accepted)

Submitted to ApJ

ABSTRACT

We present a new iron abundance analysis of the hyper metal-poor star HE 1327–2326, based on Fe II lines detected in its UV spectral range for the first time. In a Cosmic Origins Spectrograph (COS) spectrum, five new Fe II lines could be measured. A Si I line was also detected for the first time. We determine a 1D Local Thermodynamic Equilibrium (LTE) Fe II abundance of $[\text{Fe II}/\text{H}] = -5.99 \pm 0.25$. We also investigate departures from LTE for both Fe I and Fe II lines. Guided by 3D Non-LTE (NLTE) analyses of other well-studied metal-poor stars, we identify potential “residual” 3D effects in HE 1327–2326 arising from the absence of full 3D NLTE Fe calculations. Accordingly, we employ measurements of 10 weak Fe I lines previously detected in an optical spectrum of HE 1327–2326, as no Fe I lines are detectable in our UV spectrum. Following our previous work, we adopt the 1D NLTE Fe I abundance of $[\text{Fe}/\text{H}] = -5.20 \pm 0.12$ for HE 1327–2326. Adopting a value based on the optical Fe I rather than UV lines was heavily informed by our extensive investigation of model atmosphere and radiative transfer effects on different lines across the entire UV-optical wavelength range. An iron abundance of $[\text{Fe}/\text{H}] = -5.20 \pm 0.12$ is only 0.2 dex higher than what was used in previous studies. Accordingly, no previous conclusions regarding the nature of the star are affected.

Keywords: line: formation — stars: abundances — stars: Population II — stars: individual (HE 1327–2326)

Corresponding author: Rana Ezzeddine
ranae@mit.edu

* Based on observations made with the NASA/ESA Hubble Space Telescope, obtained at the Space Telescope Science Institute (STScI), which is operated by the Association of Universities for Research in Astronomy, Inc. (AURA) under NASA contract NAS 5-26555. These observations are associated with program GO-14151.

1. INTRODUCTION

The most metal-poor stars are the local equivalents to the high-redshift Universe. They retain the chemical composition of the interstellar medium at the time and place of their birth. In their atmospheres, they thus carry imprints of the nucleosynthetic signatures of their progenitor stars. Comparing the abundance signatures of Hyper and Ultra Metal-Poor (HMP and UMP) stars (with $[\text{Fe}/\text{H}] \leq -5.0$ and $-5.0 < [\text{Fe}/\text{H}] \leq -4.0$, respectively) (Beers & Christlieb 2005), to low-metallicity supernovae yields, provide unique empirical constraints on the properties of their progenitors (such as masses and explosion energies), which are thought to be Population III first stars (Frebel & Norris 2015). Also, abundance ratios such as $[\text{C}/\text{Fe}]$ in these stars can be used to constrain formation scenarios of early low-mass stars (Frebel et al. 2007; de Bannassuti et al. 2017; Ji et al. 2014).

Galactic halo metal poor stars with $[\text{Fe}/\text{H}] < -4.0$ are however difficult to identify, but decades of searches (Beers & Christlieb 2005; Frebel & Norris 2015) have delivered ~ 30 such stars (e.g., Christlieb et al. 2004; Caffau et al. 2012; Bonifacio et al. 2015; Frebel et al. 2015; Keller et al. 2014; Meléndez et al. 2016; Aguado et al. 2018a,b).

All metal-poor stars have been studied using optical spectra because spectral lines of the chemical elements of interest are found there. However, in the case of HMP and UMP stars, the absorption lines generally are weak (1-20 mÅ), that they can only be detected in extremely high quality spectra, if at all. For iron in particular, Fe II lines are even weaker than Fe I lines. In the case of HE 1327–2326, 10 Fe I lines had been previously detected in the optical spectrum of HE 1327–2326 (Frebel et al. 2008) from which an iron abundance of $[\text{Fe}/\text{H}](1\text{D, LTE}) = -5.7 \pm 0.2$ was determined (Frebel et al. 2008), under the assumption of 1D

model atmospheres and local thermodynamic equilibrium (LTE). But no Fe II lines could be detected. Both species together are commonly used to determine spectroscopic stellar atmospheric parameters e.g., via the ionization balance method (i.e., surface gravities, $\log g$), and Fe abundances, $[\text{Fe}/\text{H}]$. This highlights the importance of having at least 1-2 Fe II lines available to ensure proper stellar parameter determination.

For brighter stars, such high-quality data can sometimes be obtained in reasonable amounts of observing time but in the majority of the cases, sufficient data is out of reach. However, one alternative to obtain Fe II line measurements is from UV spectra if the stars are, once again, bright enough for such observation e.g., with the spectrographs on board the *Hubble Space Telescope* (*HST*). In the near-UV range, several Fe II lines exist that are stronger than all of those potentially available in the optical regime.

HE 1327–2326 (Frebel et al. 2005) is the second brightest star ($V = 13.5$) with $[\text{Fe}/\text{H}] < -4.0$ after J1808–5104 (Meléndez et al. 2016) ($V = 11.9$), although the former is ~ 10 times more metal-poor. Being one of the most iron-poor stars known to date makes it a very suitable target for studying the properties of the first stars and supernovae (SNe). We thus present the first detection of five Fe II lines in UV spectrum of HE 1327–2326 obtained with the Cosmic Origins Spectrograph (COS) on board the *HST*, as well as one line for Si I. With having available Fe II lines for the first time for this star, important constraints for the gravity, and thus its evolutionary status can be obtained, as well as its iron abundance.

2. OBSERVATIONS AND DATA REDUCTION

HST/COS observations of HE 1327–2326 (Program ID: GO-14151) were obtained using the G225M grating resulting in high resolving power of $R \approx 20,000$. The three UV spectral

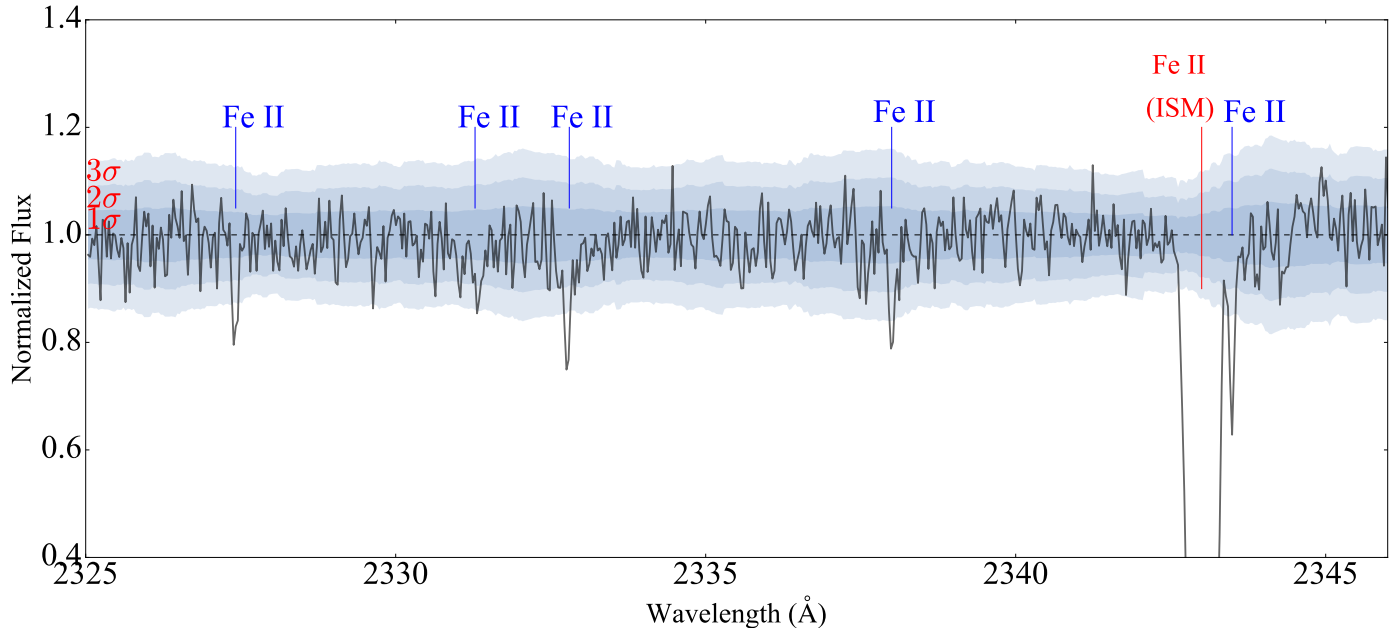


Figure 1. Selected regions of the HE 1327–2326 stacked UV spectrum where Fe II atomic lines were detected. The different blue shaded regions represent the 1σ (blue), 2σ (light blue) and 3σ (lightest blue) detection limits, respectively, as indicated.

sub-ranges $\lambda 2118 - 2151 \text{ \AA}$, $\lambda 2216 - 2249 \text{ \AA}$ and $\lambda 2315 - 2348 \text{ \AA}$ were covered by the data (for details of the COS instrument and performance we refer to reader to [Osterman et al. 2011](#)).

The total integration time was ~ 80.4 ks. The spectra were reduced with a custom reduction using a fixed extraction box height of 9 pixels in the cross-dispersion direction, recommended by the STScI¹ COS instrument team ([Snyder & Sonnentrucker 2017](#)), in order to optimize the signal-to-noise (S/N) ratio of the data. Before stacking any frames, each was individually normalized and radial velocity shifted relative to the detected Fe II line at $\lambda 2332 \text{ \AA}$. The two stripes not containing this line were shifted with the same velocity as the one with the detected line because they belong to the same exposure. All frames for each stripe were then co-added into three final spectra. The final average S/N ratios are $\sim 10 \text{ pixel}^{-1}$ near 2120 \AA and

$\sim 20 \text{ pixel}^{-1}$ near 2350 \AA . We show the part of the UV spectrum where Fe II lines are detected in Figure 1. An interstellar Fe II line at 2344 \AA is also detected, but fortunately is sufficiently shifted away from the stellar lines. Similar ISM absorption lines such those of Na I and Ca II have been previously found in the optical spectrum of HE 1327–2326 ([Frebel et al. 2005](#); [Aoki et al. 2006](#)).

3. STELLAR PARAMETERS

In a previous study, [Frebel et al. \(2005\)](#) used color-effective temperature relations from [Alonso et al. \(1996\)](#) to determine an effective temperature for HE 1327–2326 of $T_{\text{eff}} = 6180 \pm 80 \text{ K}$ from broadband *UBVRI* photometry. They then used a 12 Gyr isochrone ([Kim et al. 2002](#)) with a metallicity of $[\text{Fe}/\text{H}] = -3.5$ to constrain the gravity. Two evolutionary states were possible, $\log g=3.7$ for a subgiant, and $\log g=4.5$ for a dwarf case. To distinguish between these values, [Korn et al. \(2009\)](#) carried out a NLTE Ca I/Ca II ionization equilibrium analysis. The result favored the sub-

¹ Space Telescope Science Institute
<http://www.stsci.edu/>

giant scenario over the dwarf case. They also argued for subgiant scenario taking into account Balmer line fitting. This was reaffirmed by Mashonkina et al. (2017), who used updated Ca I atomic data in their NLTE analysis, and also found a better agreement between Ca I and Ca II for $\log g=3.7$. We re-investigate this issue using the recent parallax measurement (0.8879 ± 0.0235 mas) from the Gaia mission (DR2; Gaia Collaboration et al. 2018). We derive $\log g = 3.4 \pm 0.3$ using fundamental relations, and adopting a stellar mass of $0.7 M_{\odot}$. This, once again, confirms the subgiant scenario as the actual evolutionary status for HE 1327–2326.

For our new UV-based analysis of HE 1327–2326, we adopt $T_{\text{eff}}=6180$ K, $\log g=3.7$ and a microturbulent velocity of $\xi_t=1.7$ km s⁻¹, following Frebel et al. (2005). Accordingly, a 1D model atmospheres from Castelli & Kurucz (2004) was constructed, with input model metallicity of $[\text{Fe}/\text{H}] = -5.0$. An α -enhancement of $[\alpha/\text{Fe}] = +0.4$ was employed throughout, following tests about the impact of the chosen α -enhancement on the final iron abundances (Ezzeddine et al. 2017).

4. Fe I AND Fe II ABUNDANCES OF HE 1327–2326

4.1. Fe II abundance from UV lines

The equivalent widths (EW) of Fe II lines in the UV spectrum were measured by convolving the COS line-spread functions (Ghavamian et al. 2009) with Gaussian profiles following Roederer et al. (2016) and fitting them to the lines. The uncertainties on the equivalent widths and abundance measurements were determined by altering the continuum placement and the full-width half maximum (FWHM) of the corresponding lines by $\pm 1\sigma$, and recording the corresponding abundance changes. The significance of the detections were assessed by dividing the equivalent width of each line by its

uncertainty. Four Fe II lines at 2327 Å, 2332 Å, 2338 Å and 2343 Å were detected with $> 3\sigma$ significance, and one Fe II line at 2331 Å was detected with 2.1σ . The Fe II lines as well as the 1σ , 2σ and 3σ detection limits are shown in Figure 1. The atomic properties of the Fe II lines (excitation potential, oscillator strengths $\log gf$) and measured equivalent widths are listed in Table 1.

Line-by-line iron abundances for HE 1327–2326 were then calculated using the 2017 version of the LTE radiative transfer code MOOG² (Snedden 1973) which includes Rayleigh scattering treatment as described by Sobek et al. (2011). Custom spectroscopic analysis software first described in Casey (2014) was used. From the four Fe II lines with $> 3\sigma$ detections, we determine an average Fe II abundance of $[\text{Fe II}/\text{H}](\text{LTE}) = -5.99 \pm 0.25$ in LTE and $[\text{Fe II}/\text{H}](\text{NLTE}) = -6.01 \pm 0.25$ in NLTE. The abundance uncertainties were derived following the same procedure as that used to derive the equivalent width uncertainties. The abundances (here and throughout the rest of this paper) are reported relative to the reference Fe Solar abundance $\log \epsilon(\text{Fe})_{\odot} = 7.50$ from Asplund et al. (2009).

4.2. Are there systematic abundance differences from optical and UV Fe lines?

Using 10 Fe I lines measured in a high resolution VLT/UVES³ spectrum, Frebel et al. (2008) determined an Fe I abundance of $[\text{Fe I}/\text{H}] = -5.71 \pm 0.2$ for $\log g=3.7$. They also obtained $[\text{Fe I}/\text{H}] = -6.01 \pm 0.2$ from a 3D LTE analysis, following (Collet et al. 2005). In Ezzeddine et al. (2017), 1D LTE and 1D NLTE analyses were performed for HE 1327–2326 from

² <https://www.as.utexas.edu/~chris/moog.html>

³ The Ultraviolet and Visible Echelle Spectrograph (UVES) on the Very Large Telescope (VLT) at the European Southern Observatory on Cerro Paranal in the Atacama Desert.

Table 1. Atomic properties of the Fe II absorption lines detected in the UV spectrum of HE 1327–2326, including the excitation potentials of their lower energy levels (χ), oscillator strengths ($\log gf$), equivalent widths with their uncertainties (EW and σEW) as well as their detection significance (see Section 4.1 for details). The last column shows our result for the determined line abundances (in LTE) at $\log g=3.7$.

Absorption line	λ (Å)	χ (eV)	$\log gf$	EW (mÅ)	σEW (mÅ)	detection significance	$\log \epsilon(X)$ (dex)
Fe II	2327.39	0.08	-0.67	30.8	7.8	3.9σ	1.65
Fe II	2331.30	0.23	-0.68	18.0	8.5	2.1σ	1.43
Fe II	2332.79	0.04	-0.19	33.7	8.7	3.9σ	1.34
Fe II	2338.00	0.10	-0.43	32.5	8.8	3.7σ	1.46
Fe II	2343.49	0.00	+0.06	53.8	10.3	5.2σ	1.56

which $[\text{Fe I}/\text{H}](\text{NLTE}) = -5.20 \pm 0.20$ and $[\text{Fe I}/\text{H}](\text{LTE}) = -5.80 \pm 0.16$ were obtained, using the same lines as Frebel et al. (2008). The LTE optical Fe I abundance agrees within uncertainties (~ 0.15 dex) with our new UV LTE Fe II abundance, suggesting no offset as a function of a wavelength when considering LTE.

Our NLTE “abundance correction” obtained for Fe II, defined by the difference between the average NLTE abundance and the corresponding average LTE abundance, $\Delta_{\text{corr}} = \log \epsilon(\text{NLTE}) - \log \epsilon(\text{LTE})$, is negligible ($\Delta_{\text{corr}} = -0.02$ dex). This result is in line with previous studies (Mashonkina et al. 2011; Bergemann et al. 2012; Amarsi et al. 2016; Ezzeddine et al. 2017), as NLTE line strengths and abundances of dominant species, i.e., Fe II, are not theoretically expected to significantly deviate from the LTE assumption.

Comparing this NLTE Fe II abundance with the NLTE optical Fe I result reveals it to be higher than that inferred from the UV Fe II lines, by $\Delta(\log \epsilon(\text{Fe I, NLTE}) - \log \epsilon(\text{Fe II, NLTE})) = 0.81$ dex. This difference between the optical and UV abundances in NLTE is largely due to the significant deviations of the NLTE Fe I

abundance from the LTE assumption, namely by $\Delta_{\text{corr}} \sim 0.6$ dex (Ezzeddine et al. 2017). Such a large discrepancy between Fe I and Fe II can not possibly be compensated by increasing $\log g$ to attain ionization equilibrium, as it would lead to non-physical surface gravity values, i.e., $\log g \sim 6$.

4.3. Previous optical vs UV studies

Discrepancies between the optical and UV abundances of the same species have been reported by previous studies (Roederer et al. 2012; Lawler et al. 2013; Roederer et al. 2014a,b,c). These studies found that the abundances of individual UV lines show larger scatter than those of the optical lines (up to ± 0.4 dex around the mean), and that the mean UV Fe abundances are slightly lower in the UV than in the optical (i.e., slight negative trends with decreasing wavelengths). Roederer et al. (2012), for example, studied the LTE iron abundances in the UV and optical spectra of four reference metal-poor stars with $[\text{Fe}/\text{H}] > -3.1$. They found lower average abundances down to -0.2 dex for lines lying between ~ 3100 and 3700 Å, compared with those at $\lambda > 4000$ Å.

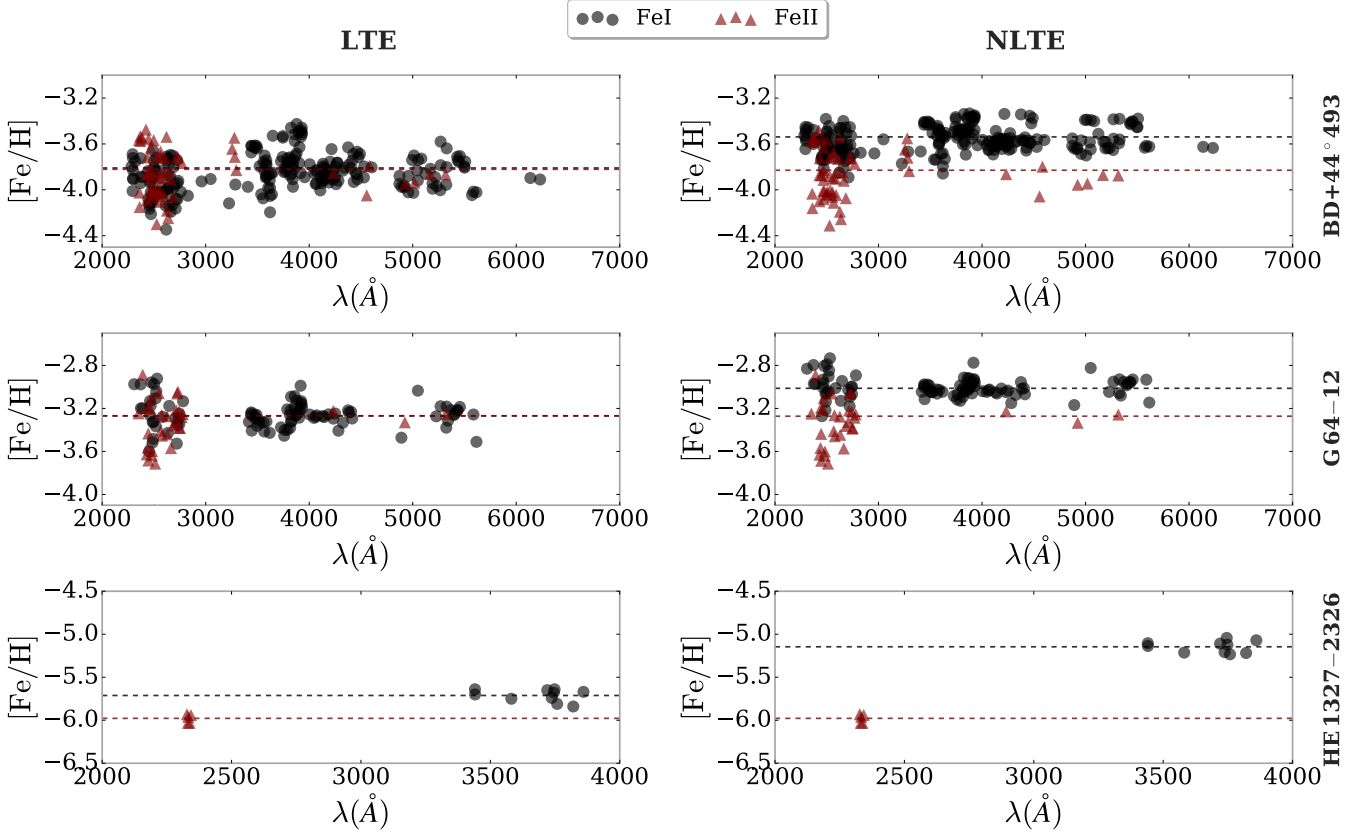


Figure 2. FeI and FeII line-by-line LTE and NLTE abundances for G 64–12, BD+44°493 and HE 1327–2327 as a function of wavelength.

In most of these studies, however, the Fe I lines did not continuously cover the entire wavelength range from the UV to the optical, especially toward the lowest $\lambda \sim 2000 \text{ \AA}$, to draw firm conclusions. It was suggested that the source of these discrepancies and decreasing abundance trends towards UV wavelengths (for the same chemical species) might be due to either NLTE effects or the underestimation of the H I contribution to the continuum opacities, which becomes important toward the lower UV wavelengths at $\lambda < 3500 \text{ \AA}$. For more details on these suggestions, we refer the reader to Figure 11 in [Roederer et al. 2012](#). However, as we show above, NLTE abundances only appear to make any discrepancies even larger.

4.4. Investigating optical-UV abundance discrepancies with the well-studied metal-poor stars G 64–12 and BD +44° 493

We principally investigate the origin of the abundance discrepancies between lines found in the optical and UV wavelength range in HE 1327–2326 and previous studies. For that, we performed a new detailed LTE and NLTE abundance analyses of two well studied extremely metal-poor stars, G 64–12 and BD +44°493. Both stars have sufficient Fe I and Fe II lines available across large regions of the optical and UV spectra. For G 64–12, we used *EW* measurements of UV and optical Fe lines obtained from *HST*/STIS⁴ and *VLT*/UVES

⁴ Space Telescope Imaging Spectrograph on the *HST* (Program ID GO-9049).

spectra⁵, respectively (Roederer et al. 2018). We adopt $T_{\text{eff}} = 6492\text{K}$ and $\log g = 4.4$ as well as $[\text{Fe}/\text{H}] = -3.2$ and $\xi_t = 1.5\text{km/s}$ for input stellar parameters from Roederer et al. (2018). Their T_{eff} agrees well with the Infrared Flux Method (IRFM) (Casagrande et al. 2010) value of $6464 \pm 150\text{K}$. Their surface gravity also agrees, within uncertainties, to that derived from the Gaia DR2 parallax ($3.7625 \pm 0.0855\text{mas}$) of $\log g = 4.1 \pm 0.3$.

For BD +44°493, we used published *EW* measurements for UV and optical Fe lines from Ito et al. (2013) and Placco et al. (2014), respectively. We adopt stellar atmospheric parameters from Ito et al. (2013), with $T_{\text{eff}} = 5430\text{K}$ determined from the IRFM (Casagrande et al. 2010), $\log g = 3.4$, $[\text{Fe}/\text{H}] = -3.8$ and $\xi_t = 1.3\text{km/s}$ from a spectroscopic Fe I/Fe II abundance analysis. The Gaia DR2 parallax ($4.7595 \pm 0.0659\text{mas}$) yields a surface gravity of $\log g = 3.5 \pm 0.3$, which is in very good agreement with the value from Ito et al. (2013).

NLTE calculations were performed following the same procedure in Ezzeddine et al. (2017), where the NLTE radiative transfer code MULTI2.3 (Carlsson 1986, 1992) was used with the MARCS (Gustafsson et al. 1975, 2008; Plez 2012) model atmospheres interpolated to the corresponding stellar parameters. The LTE abundances were also calculated using the same code and atmospheric models. The average abundance results obtained for G 64–12, BD +44°493 and HE 1327–2326 from optical and UV Fe I and Fe II lines (whenever possible) are displayed in Table 2. Line-by-line abundances as a function of wavelengths are also shown for the three stars in Figure 2.

In LTE, no systematic differences are found between the abundances derived from the

UV and optical lines or those derived from Fe I and Fe II lines for BD +44°493, G 64–12 and HE 1327–2326. Any small differences are within the abundance uncertainties of the three stars. In NLTE, however, the abundances obtained from both optical and UV Fe I lines are systematically higher than those from the Fe II lines from either region (when available). The Fe I-Fe II discrepancies are +0.30 dex for BD +44°493, +0.33 dex for G 64–12 and +0.80 dex for HE 1327–2326. It is important to note, though, that the abundances inferred from UV Fe II lines show larger scatter (± 0.2 dex for G 64–12 and BD +44°493) around the mean values as compared to those inferred from optical Fe II lines (± 0.14 dex for BD +44°493 and ± 0.05 dex for G 64–12), or UV and optical Fe I lines ($\sim \pm 0.15$ dex). The same large scatter is obtained in both LTE and NLTE analyses. This is in line with previous LTE Fe abundance studies based on UV lines (e.g., Roederer et al. 2012).

In order to further understand this discrepancy, we considered other studies on e.g. G 64–12. Amarsi et al. (2016) performed a full 3D NLTE abundance analysis for G 64–12 and three other well-studied metal-poor stars. As part of their work, they found their 1D NLTE abundances for G 64–12 to be higher than the 1D LTE values, up to 0.23 dex for Fe I but are, of course, negligible for Fe II. This is very similar to our findings ($\Delta_{\text{corr}} = 0.25$ dex.), albeit using a slightly lower $\log g$ value by 0.14 dex than ours.

Also, Amarsi et al. (2016) compared 3D NLTE and 1D NLTE abundances in G 64–12. They found non-negligible positive abundance corrections of +0.16 dex for Fe II and $\sim +0.11$ dex for Fe I due to 3D effects in G 64–12. Interestingly, both these 3D NLTE Fe I and Fe II abundance are increased (although not at the same level) compared to the 1D NLTE case. This differential increase of both Fe I and Fe II abundances

⁵ Based on observations collected at the European Organisation for Astronomical Research in the Southern Hemisphere under ESO programme 67.D-0554(A) (PI = Christlieb).

Table 2. LTE and NLTE average line Fe I and Fe II abundances of the test comparison stars BD +44°493 and G 64–12 as well as HE 1327–2326, determined from their UV and optical spectra respectively.

	BD +44°493		G 64–12		HE 1327–2326	
	LTE	NLTE	LTE	NLTE	LTE	NLTE
[Fe I/H] ^{OP}	-3.81 ± 0.15	-3.54 ± 0.10	-3.27 ± 0.10	-3.02 ± 0.10	-5.80 ± 0.16	-5.20 ± 0.12
[Fe II/H] ^{OP}	-3.83 ± 0.14	-3.83 ± 0.14	-3.27 ± 0.05	-3.27 ± 0.05
[Fe I/H] ^{UV}	-3.95 ± 0.15	-3.61 ± 0.13	-3.24 ± 0.18	-2.99 ± 0.13
[Fe II/H] ^{UV}	-3.86 ± 0.20	-3.87 ± 0.21	-3.34 ± 0.20	-3.34 ± 0.21	-5.99 ± 0.25	-6.01 ± 0.25
[Fe I/H] ^{OP+UV}	-3.85 ± 0.16	-3.56 ± 0.11	-3.26 ± 0.16	-3.01 ± 0.10	-5.80 ± 0.16	-5.20 ± 0.12
[Fe II/H] ^{OP+UV}	-3.86 ± 0.19	-3.86 ± 0.19	-3.33 ± 0.15	-3.34 ± 0.12	-5.99 ± 0.26	-6.01 ± 0.25

brings them into agreement with each other, to within ~ 0.1 dex, when abundance uncertainties are also ~ 0.1 dex.

The abundances derived in this combined 3D NLTE framework furthermore suggests Fe I and Fe II corrections to increase even more toward lower metallicities relative to just 1D NLTE (Amarsi et al. 2016; Nordlander et al. 2017). This behavior has already been documented as part of the full 3D NLTE analysis of the most-iron poor giant star SMSS 0313–6708 with $[\text{Fe}/\text{H}] < -7.0$ (Nordlander et al. 2017). “Residual” 3D corrections of $\Delta^{3\text{D}} = \log \epsilon(3\text{D}, \text{NLTE}) - \log \epsilon(1\text{D}, \text{NLTE}) = 0.2$ dex were determined for a putative Fe I line in this star. Moreover, the corresponding residual 3D correction for Fe II lines in SMSS 0313–6708 is expected to be larger than that for Fe I (Amarsi et al. 2016), although, unfortunately, no explicit calculations were reported for SMSS 0313–6708. In addition, they report a 1D NLTE effect of $\Delta_{\text{corr}} = 0.6$ (compared to 1D LTE). This is larger than the residual 3D correction, but comparable to what we find for HE 1327–2326 in the present study. Finally, Nordlander et al. (2017) found that the 3D LTE framework can heavily underestimate the Fe I abundances by ~ 1 dex compared to the full 3D NLTE case.

Consequently, they deduced that the 3D NLTE Fe I abundance ($[\text{Fe}/\text{H}] < -6.53 \pm 0.5$) is

the best avenue for determining the iron abundance of this star, but if a 3D analysis is not possible, the 1D NLTE case ($[\text{Fe}/\text{H}] < -6.73 \pm 0.2$) provides a robust estimate of the Fe abundance instead. This will be the case for most analyses, given that full 3D NLTE calculations are based on complex and lengthy computational requirements.

By analogy, we thus conclude that the discrepancies observed in HE 1327–2326 between the UV Fe II line and the optical Fe I line abundances may well be due to these unaccounted 3D residual corrections. Further exploration of the issue in terms of 3D modeling is warranted, but beyond the scope of the present study.

4.5. Adopted iron abundance of HE 1327–2326

Our investigation into understanding the differences obtained between the abundances of Fe I and Fe II arising from LTE, NLTE and 3D calculations for G 64–12, BD +44°493 and SMSS 0313–6708 yielded that the 1D NLTE Fe I abundance is presently the most robust indicator to use, if a full 3D NLTE calculation is not available (Amarsi et al. 2016; Nordlander et al. 2017).

Guided by these results, for HE 1327–2326, we thus adopt the 1D NLTE abundance of $[\text{Fe}/\text{H}] = -5.20 \pm 0.12$ inferred from optical Fe I lines as our final $[\text{Fe}/\text{H}]$ value. This new re-

sult is slightly higher than what was previously adopted $[\text{Fe}/\text{H}] = -5.4$ (Frebel et al. 2005), which was an LTE value corrected with an arbitrarily chosen NLTE correction of 0.2 dex. A value of $[\text{Fe}/\text{H}] = -5.2$ should be more physically meaningful for any interpretation of the origin of this star and its abundance pattern than any other values. Performing a computationally challenging full 3D NLTE abundance analysis in the future would hopefully show agreement between the abundances of both Fe I and Fe II species, within uncertainties.

5. SILICON UV ABUNDANCE

In addition to the Fe II lines, we also detected for the first time a Si I line at 2124.12 Å in the UV spectrum of HE 1327–2326. From that, using the same procedure as for Fe II reported in Section 4, we determine a Si abundance of $[\text{Si}/\text{H}] = -4.51 \pm 0.23$.

The UV Si abundance is higher than the optical upper limit reported by Ji et al. (2014) of $[\text{Si}/\text{H}] = -5.40$. These authors investigated the role of critical gas fragmentation in first low-mass stars formation and compared their models to abundance measurements of Si in UMP stars. Their upper limit falls right below that of the supernova shock dust size distribution limit (see Figure 5 in Ji et al. 2014). The implication was previously that HE 1327–2326 could not have formed from gas solely cooled by silicon-based dust, but instead by some other mechanism that enables low-mass star formation.

At face value, our new $[\text{Si}/\text{H}]$ measurement only places HE 1327–2326 below the standard shock dust size distribution limit which is higher than the supernova shock dust distribution. Assuming that no discrepancies exist between the Si abundances inferred from UV and optical lines, this would suggest that the formation HE 1327–2326 (and perhaps that of other UMP stars) from early gas clouds could have been driven by dust-induced gas cooling although the high carbon abundance of HE 1327–2326 still

points to a formation from fine-structure line cooled gas (Frebel et al. 2007).

6. SUMMARY

We analyzed the UV spectrum of HE 1327–2326 between 2120 and 2360 Å, in which 5 new Fe II lines as well as one Si I line have been detected. We obtain a 1D LTE Fe II abundance of $[\text{Fe II}/\text{H}] = -5.99 \pm 0.25$ from the four Fe II lines with $> 3\sigma$ detection significance. This value is ~ 0.8 dex lower than the 1D NLTE iron abundance inferred from optical Fe I lines of $[\text{Fe}/\text{H}] = -5.20 \pm 0.12$. We investigated previous claims that discrepancies exist between abundances inferred from UV and optical lines using the two well-studied metal-poor stars BD +44°493 and G 64–12. We find that no systematic differences are found in LTE when sufficient UV and optical lines are used in the analysis, however, Fe II abundances of UV lines display larger scatter from the mean values than their optical counterparts. On the other hand, non-negligible differences are found between abundances inferred from Fe I and Fe II lines in NLTE in both stars, as is the case for HE 1327–2326. These differences could be attributed to “residual” 3D effects, as discussed in Section 4.4.

We therefore adopt the 1D NLTE iron abundance of $[\text{Fe}/\text{H}] = -5.20 \pm 0.12$ as the final iron abundance of HE 1327–2326. This value can be considered as best possible if a full 3D NLTE calculation is lacking. This follows recommendations by Nordlander et al. (2017) who performed both 1D and 3D NLTE analyses in an HMP star.

This iron abundance in HE 1327–2326 is just 0.2 dex higher than of $[\text{Fe}/\text{H}] = -5.40 \pm 0.2$ adopted by Frebel et al. (2005). They used this latter value in comparing the overall elemental abundance ratio pattern of HE 1327–2326 (relative to Fe) to supernovae explosion nucleosynthesis yields of Population III stars, in order to derive its progenitor star properties. Such a

negligible difference between our values, relative to the full abundance scale spanning over 6 dex (See Figure 2 in [Frebel et al. 2005](#)), does not alter the conclusions deduced by their results, which are still expected to hold.

We thank the anonymous referee for their time and useful comments which helped improve this manuscript. We thank Ian U. Roederer for the useful discussion and advice on this work, and for providing the equivalent widths and stellar parameters measurements of G 64–12 as well as the equivalent widths for HE 1327–2326. R.E. acknowledges support from a JINA-CEE fellowship (Joint Institute for Nuclear Astrophysics - Center for the Evolution of the Elements), funded in part by the

National Science Foundation under Grant No. PHY-1430152 (JINA-CEE). A.F. is supported by NSF-CAREER grant AST-1255160. AF acknowledges support from the Silverman (1968) Family Career Development Professorship. We also thank and appreciate the expert assistance of Jason Tumlinson in the custom extraction of the UV spectra. This research has made use of NASA’s Astrophysics Data System Bibliographic Services, the arXiv pre-print server operated by Cornell University and the Atomic Spectra Database hosted by the National Institute of Standards and Technology (NIST).

Software: MOOG ([Snedden 1973](#); [Sobeck et al. 2011](#)), MULTI2.3 ([Carlsson 1986, 1992](#)), MARCS ([Gustafsson et al. 1975, 2008](#); [Plez 2012](#))

REFERENCES

- Aguado, D. S., Allende Prieto, C., González Hernández, J. I., & Rebolo, R. 2018a, *ApJL*, 854, L34
- Aguado, D. S., González Hernández, J. I., Allende Prieto, C., & Rebolo, R. 2018b, *ApJL*, 852, L20
- Alonso, A., Arribas, S., & Martínez-Roger, C. 1996, *A&A*, 313, 873
- Amarsi, A. M., Lind, K., Asplund, M., Barklem, P. S., & Collet, R. 2016, *MNRAS*, 463, 1518
- Aoki, W., Frebel, A., Christlieb, N., et al. 2006, *ApJ*, 639, 897
- Asplund, M., Grevesse, N., Sauval, A. J., & Scott, P. 2009, *ARA&A*, 47, 481
- Beers, T. C., & Christlieb, N. 2005, *ARA&A*, 43, 531
- Bergemann, M., Lind, K., Collet, R., Magic, Z., & Asplund, M. 2012, *MNRAS*, 427, 27
- Bonifacio, P., Caffau, E., Spite, M., et al. 2015, *A&A*, 579, A28
- Caffau, E., Bonifacio, P., François, P., et al. 2012, *A&A*, 542, A51
- Carlsson, M. 1986, *Uppsala Astronomical Observatory Reports*, 33
- Carlsson, M. 1992, in *Astronomical Society of the Pacific Conference Series*, Vol. 26, *Cool Stars, Stellar Systems, and the Sun*, ed. M. S. Giampapa & J. A. Bookbinder, 499
- Casagrande, L., Ramírez, I., Meléndez, J., Bessell, M., & Asplund, M. 2010, *A&A*, 512, A54
- Casey, A. R. 2014, PhD thesis, Australian National University, doi:10.5281/zenodo.49493
- Castelli, F., & Kurucz, R. L. 2004, *astro-ph/0405087*
- Christlieb, N., Gustafsson, B., Korn, A. J., et al. 2004, *ApJ*, 603, 708
- Collet, R., Asplund, M., & Thévenin, F. 2005, *A&A*, 442, 643
- de Bannassuti, M., Salvadori, S., Schneider, R., Valiante, R., & Omukai, K. 2017, *MNRAS*, 465, 926
- Ezzeddine, R., Frebel, A., & Plez, B. 2017, *ApJ*, 847, 142
- Frebel, A., Chiti, A., Ji, A. P., Jacobson, H. R., & Placco, V. M. 2015, *ApJL*, 810, L27
- Frebel, A., Collet, R., Eriksson, K., Christlieb, N., & Aoki, W. 2008, *ApJ*, 684, 588
- Frebel, A., Johnson, J. L., & Bromm, V. 2007, *MNRAS*, 380, L40
- Frebel, A., & Norris, J. E. 2015, *ARA&A*, 53, 631
- Frebel, A., Aoki, W., Christlieb, N., et al. 2005, *Nature*, 434, 871
- Gaia Collaboration, Brown, A. G. A., Vallenari, A., et al. 2018, *ArXiv e-prints*, arXiv:1804.09365

- Ghavamian, P., Aloisi, A., Lennon, D., et al. 2009, Preliminary Characterization of the Post-Launch Line Spread Function of COS, Tech. rep.
- Gustafsson, B., Bell, R. A., Eriksson, K., & Nordlund, A. 1975, *A&A*, 42, 407
- Gustafsson, B., Edvardsson, B., Eriksson, K., et al. 2008, *A&A*, 486, 951
- Ito, H., Aoki, W., Beers, T. C., et al. 2013, *The Astrophysical Journal*, 773, 33
- Ji, A. P., Frebel, A., & Bromm, V. 2014, *ApJ*, 782, 95
- Keller, S. C., Bessell, M. S., Frebel, A., et al. 2014, *Nature*, 506, 463
- Kim, Y.-C., Demarque, P., Yi, S. K., & Alexander, D. R. 2002, *ApJS*, 143, 499
- Korn, A. J., Richard, O., Mashonkina, L., et al. 2009, *ApJ*, 698, 410
- Lawler, J. E., Guzman, A., Wood, M. P., Sneden, C., & Cowan, J. J. 2013, *ApJS*, 205, 11
- Mashonkina, L., Gehren, T., Shi, J.-R., Korn, A. J., & Grupp, F. 2011, *A&A*, 528, A87
- Mashonkina, L., Sitnova, T., & Belyaev, A. K. 2017, *A&A*, 605, A53
- Meléndez, J., Placco, V. M., Tucci-Maia, M., et al. 2016, *A&A*, 585, L5
- Nordlander, T., Amarsi, A. M., Lind, K., et al. 2017, *A&A*, 597, A6
- Osterman, S., Green, J., Froning, C., et al. 2011, *Ap&SS*, 335, 257
- Placco, V. M., Beers, T. C., Roederer, I. U., et al. 2014, *ApJ*, 790, 34
- Plez, B. 2012, Turbospectrum: Code for spectral synthesis, Astrophysics Source Code Library, , , ascl:1205.004
- Roederer, I. U., Jacobson, H. R., Thanathibodee, T., Frebel, A., & Toller, E. 2014a, *ApJ*, 797, 69
- Roederer, I. U., Placco, V. M., & Beers, T. C. 2016, *The Astrophysical Journal Letters*, 824, L19
- Roederer, I. U., Preston, G. W., Thompson, I. B., et al. 2014b, *AJ*, 147, 136
- Roederer, I. U., Sneden, C., Lawler, J. E., et al. 2018, *ApJ*, 860, 125
- Roederer, I. U., Lawler, J. E., Sobeck, J. S., et al. 2012, *ApJS*, 203, 27
- Roederer, I. U., Schatz, H., Lawler, J. E., et al. 2014c, *ApJ*, 791, 32
- Sneden, C. A. 1973, PhD thesis
- Snyder, E., & Sonnentrucker, P. 2017, "Analysis of the COS/NUV Extraction Box Heights", STScI
- Sobeck, J. S., Kraft, R. P., Sneden, C., et al. 2011, *AJ*, 141, 175